SUPPLEMENTAL MATERIAL

Khalaj et al., https://doi.org/10.1084/jem.20161595

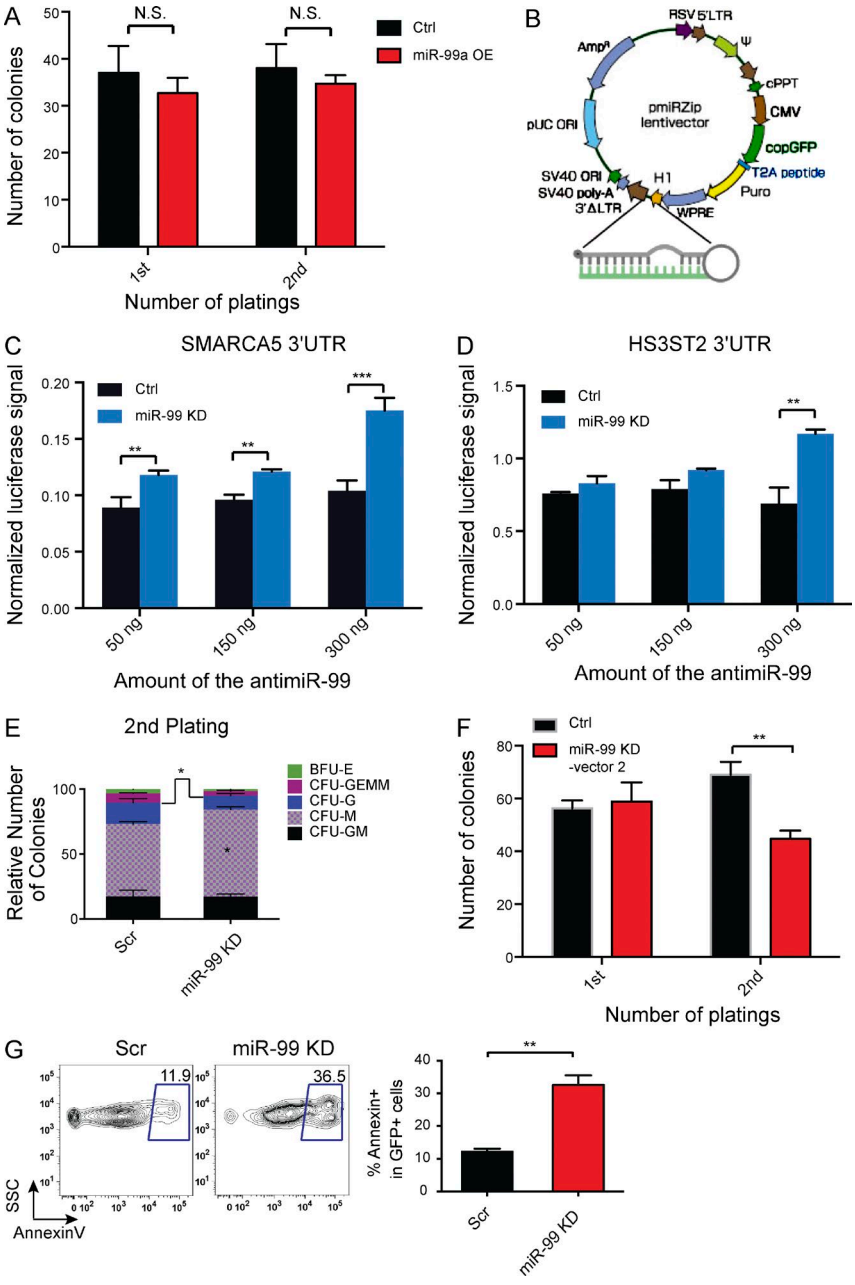

Figure S1. **In vitro studies of HSPCs following *miR-99* KD or overexpression.** (A) Lentiviral overexpression of *miR-99* does not affect colony formation efficiency of LT-HSC in methylcellulose colony assays. Data represent mean count ± SEM (Student's *t* test; $n = 3$) and are representative of two independent experiments. (B) Schematic of the lentiviral miR-Zip vector used for *miR-99* KD experiments (Systems Biosciences [SBI]). (C and D) Luciferase assay shows anti–*miR-99* (Zip-99) can release *miR-99*–mediated suppression of its targets in a dose-dependent manner. 293T cells were transfected with different doses of the Zip-99 vector along with luciferase vectors harboring 3′ UTRs of the known *miR-99* targets *SMARCA5* (B) and *HS3ST2* (C) downstream of a luciferase gene. All samples were simultaneously transfected with 50 ng of the *miR-99a*–overexpressing vector to ensure suppression of targets. 48 h after transfection, relative luciferase activity was measured. Data represent mean ± SEM (Student's *t* test; $n = 3$) and are representative of three independent experiments. (E) Colony-forming capacity of HSCs is reduced after *miR-99* KD following second plating. 15,000 GFP$^+$ cells were replated 7 d after the first plating. Colony types were scored after 7 to 10 d. Data represent mean percentage ± SEM (Student's *t* test; $n = 3$) and are representative data of three independent experiments. (F) Colony-forming activity of LT-HSCs is reduced upon transduction with anti–*miR-99* vector 2. Double-sorted LT-HSC cells were cultured in methylcellulose medium and replated every 7 to 10 d. Data represent mean count ± SEM (Student's *t* test; $n = 3$) and are representative of two independent experiments. (G) HSCs transduced with anti–*miR-99* virus display increased apoptosis 7 d post-plating. 48 h after transduction, 150 GFP$^+$ cells were sorted into complete methylcellulose. 7 d later, the resulting GFP+ cells were analyzed for Annexin V staining. Data represent mean percentage ± SEM (Student's *t* test; $n = 2$) and are representative of two independent experiments. **, $P < 0.01$; ***, $P < 0.001$.

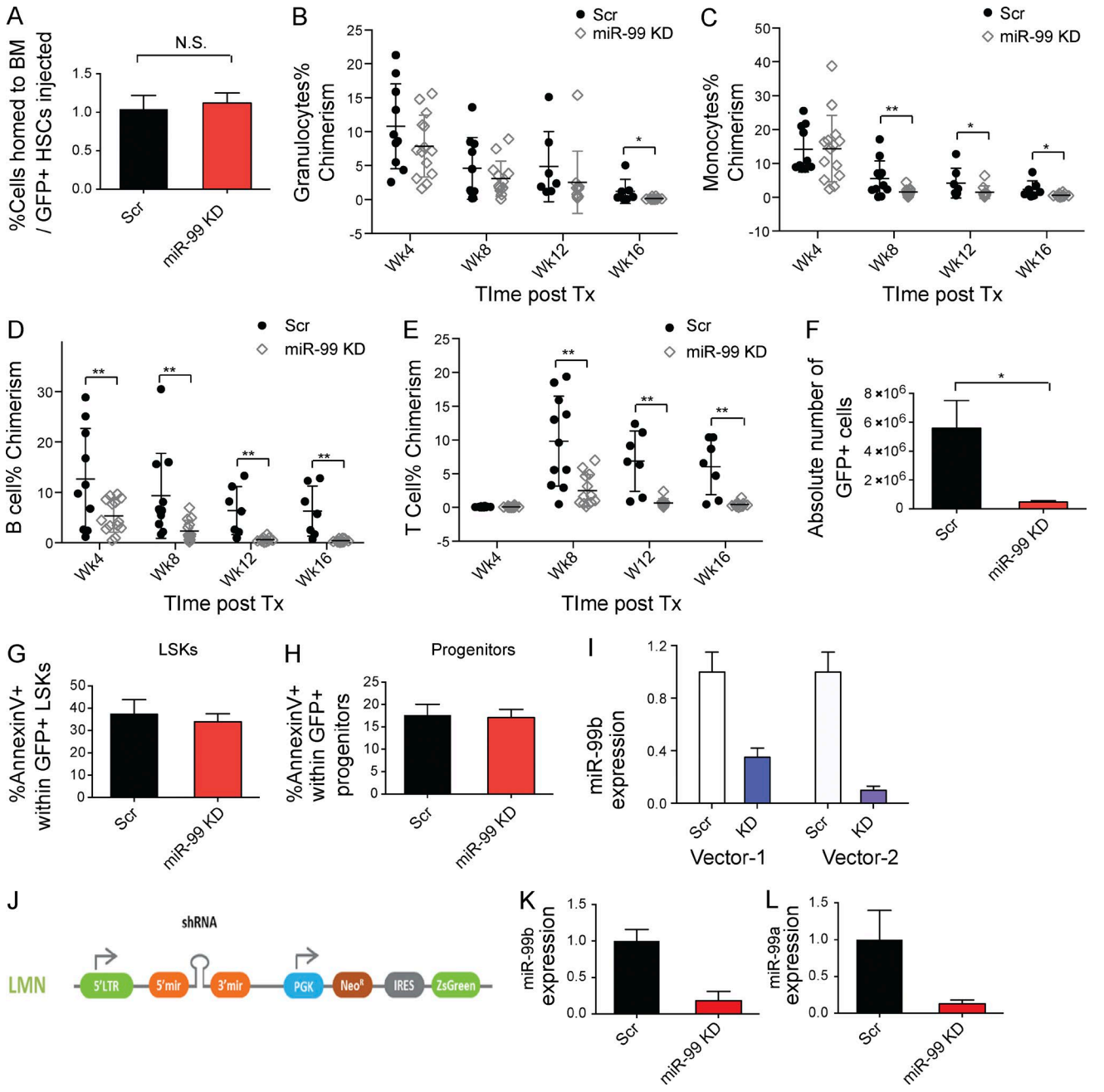

Figure S2. **In vivo characterization of *miR-99* KD HSCs and functional validation of *miR-99* KD vectors.** (A) Homing of LT-HSCs into the BM after transplantation. 5,000 GFP$^+$ LT-HSCs were transplanted into lethally irradiated animals. 24 h later, all long bones, hips, and spine were analyzed for the presence of donor cells. Data represent mean absolute counts ± SEM (n = 3 for Scr and n = 4 for *miR-99* KD mice). (B–E) GFP$^+$ chimerism within total granulocytes (B), monocytes (C), B cells (D), and T cells (E) in the peripheral blood at 4 to 16 wk post-transplantation of *miR-99* KD LT-HSCs. Data represent mean percentage ± SD (Student's t test; n = 11 for Scr and n = 14 for *miR-99* KD) and are representative of two independent experiments. (F) GFP$^+$ engraftment in the BM 16 wk after transplantation of LT-HSCs following *miR-99* KD. Data represent mean count ± SEM (Student's t test; n = 4) and are representative of two independent experiments. (G and H) Annexin V staining of GFP$^+$ LSK (G) and progenitor (H) cells in the BM 6 mo post-transplant. Data represent mean percentage ± SEM (Student's t test; n = 7 for Scr and n = 8 for *miR-99* KD) and are representative of two independent experiments. (I) Quantimir quantitative RT-PCR analysis of *miR-99b* expression 48 h post-transduction of MonoMac6 AML cells with the two anti–*miR-99* vectors. Expression was normalized to *miR-16*. Data represent mean ratio ± SD (Student's t test; n = 3) and are representative of three independent experiments. (J) Schematic diagram of the *miR-30*–based LMN retroviral vector used for *miR-99* KD experiments in MLL-AF9 mice. (K and L) Expression of *miR-99b* and *miR-99a* after transduction of MLL-AF9+–overexpressing LSK cells with the retroviral *miR-99* KD vector. Data represent mean ratio ± SD (Student's t test; n = 3) and are representative of three independent experiments. *, $P < 0.05$; **, $P < 0.01$.

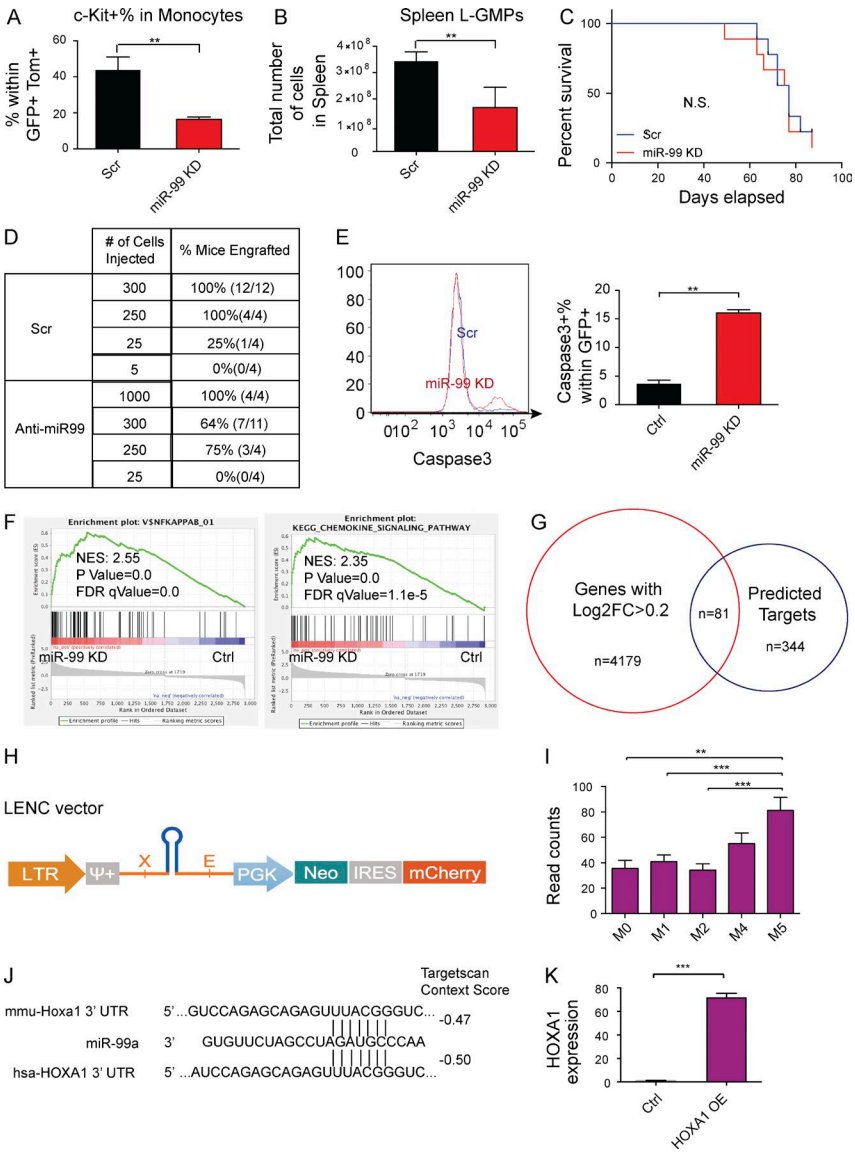

Figure S3. **In vivo characterization of *miR-99* KD MLL-AF9 AML transplated mice and identification of *miR-99* targets.** (A) Flow cytometry analysis of c-Kit expression in $Gr1^{neg}Mac1^{+}$ monocytes within the spleen of MLL-AF9^{+} AML primary transplant recipients. Expression was measured at the time of death. Mean percentage ± SEM (Student's *t* test; $n = 4$ for Scr and $n = 3$ for *miR-99* KD). Representative data from three independent experiments are shown. (B) Flow cytometry analysis of L-GMPs within the spleen of primary transplantation recipients of MLL-AF9^{+} AML. Absolute number of GFP^{+} tdTom^{+} L-GMPs was measured at the time of death. Data represent mean absolute count ± SEM (Student's *t* test; $n = 4$) and are representative of three independent experiments. (C) Kaplan–Meier survival curve for the primary MLL-AF9 transplantation experiment. 30,000 GFP+ tdTom+ LSKs cotransduced with MLL-AF9 and *miR-99* KD vectors were transplanted into sublethally irradiated C57BL/6 recipients (Mantel–Cox test; $n = 10$). (D) Limiting dilution assay on the MLL-AF9+ *miR-99* KD/Scr cells from the BM of primary transplantation recipients. Table shows the number of AML cells transplanted and percentages and numbers of mice succumbing to the disease. (E) Flow cytometry analysis of caspase-3 activation in MonoMac6 cells transduced with anti–*miR-99* 8 d post-transduction. Mean percentage ± SEM (Student's *t* test; $n = 4$). Representative data from three independent experiments are shown. (F) GSEA of LSK cells transduced with *miR-99* KD 48 h post-transduction reveals induction of the NF-κB pathway and chemokine signaling gene signatures. FDR, false discovery rate; NES, normalized enrichment score. (G) Venn diagram shows the 81 genes up-regulated in the LSK cell *miR-99* KD RNA-seq data (log_2 fold change >0.2; Fig. 6 A and Table S2 B) and also predicted to be *miR-99* targets according to TargetScan (Agarwal et al., 2015), PITA (Kertesz et al., 2007), and cBio prediction algorithms (Betel et al., 2010; Table S2 A). (H) Schematic diagram of the miR-E–based retroviral vector, LENC, used to generate the shRNA library. (I) miRNA-sequencing data for *HOXA1* expression from 153 AML patients derived from the AML TCGA database. Expression is graphed as a function of the French–American–British classification of AML. (J) Binding site of *miR-99a* to 3′ UTRs of *Hoxa1* and *HOXA1*, along with their binding energy predicted by TargetScan (Agarwal et al., 2015). (K) TaqMan quantitative RT-PCR for *HOXA1* expression with transduction of MonoMac6 cells with the *HOXA1* overexpression vector, confirming up-regulation of *HOXA1*. Expression was normalized to *ACTB*. Data represent mean ratio ± SD (Student's *t* test; $n = 3$) and are representative data of two independent experiments. **, $P < 0.01$; ***, $P < 0.001$.

Tables S1 and S2 are provided as Excel files. Table S1 lists genes up-regulated comparing LGMPs with normal GMPs. Table S2 shows RNA-Seq and DNA deep sequencing data related to the shRNA library screen.

REFERENCES

Agarwal, V., G.W. Bell, J.W. Nam, and D.P. Bartel. 2015. Predicting effective microRNA target sites in mammalian mRNAs. *eLife*. 4:e05005. http://dx.doi.org/10.7554/eLife.05005

Betel, D., A. Koppal, P. Agius, C. Sander, and C. Leslie. 2010. Comprehensive modeling of microRNA targets predicts functional non-conserved and non-canonical sites. *Genome Biol.* 11:R90. http://dx.doi.org/10.1186/gb-2010-11-8-r90

Kertesz, M., N. Iovino, U. Unnerstall, U. Gaul, and E. Segal. 2007. The role of site accessibility in microRNA target recognition. *Nat. Genet.* 39:1278–1284. http://dx.doi.org/10.1038/ng2135